Magnetic Coupling Characteristics and Efficiency Analysis of Spiral Magnetic Power Pads for Inductive WPT System

Dharavath Kishan

E-mobility research laboratory, Dept. of Electrical and Electronics Engineering, National Institute of Technology Karnataka, Surathkal, India
E-mail: kishand@nitk.edu.in

Received 18 October 2021; Accepted 02 April 2022;
Publication 24 June 2022

Abstract

The inductive wireless power transfer system (IWPT) for electric vehicle battery charging works based on the principle of mutual induction (MI). The amount of power transfer from source to vehicle battery be contingent on the mutual inductance (MI) within the inductively coupled pads. This mutual inductance depends on the type of the inductive power pads, the distance among them, their positioning etc. This paper develops and study the inductive coupling characteristics of identical spiral circular and square inductive power pads. The coupling characteristics at various misalignments with different vertical distance between the coils is presented. In this work, the inductive power pads without using ferrite bars, and with ferrite bars are considered. The coupling characteristics of the spiral circular and square are computed using FEM simulations and validated with experimental results. This paper also investigated the power loss and efficiency analysis of the spiral inductive pads of the resonant IWPT system.

Keywords: Electric vehicles, inductive wireless power transfer, magnetic power pads, mutual inductance.

Distributed Generation & Alternative Energy Journal, Vol. 37_5, 1703–1720.
doi: 10.13052/dgaej2156-3306.37517

1 Introduction

The popularity of electric vehicles (EVs) have increased since last decade due to their environmental friendliness, efficiency and reduced noise [1, 2]. Battery pack are crucial components in these vehicles and the battery packs can be charged using on-board or off board chargers that can be powered by wired/ and wireless connections. Wired connection chargers known as conductive chargers require heavy gauge cables which may be inconvenient and has potential risk hazards [3, 4]. In wireless battery charger based on inductive coupling, the energy can transfer without any physical connection over medium range distances. This type of chargers are convenient, safe and finds it use in automotive, robotics, medical implantable devices and aerospace [2–4].

In the IWPT system, the power transfer takes place between the source to load through high frequency magnetic field. The magnetic field is generated with the help of magnetic power pads which are called as transmitter (TxP) and receiver Pad (RxP). The magnitude of power transfer capability will depend on mutual inductance between magnetic power pads [5–8]. The MI will be affected due to shape and alignment of the inductive power pads of the IWPT systems. Hence, the estimation of MI is important factor in the design of IWPT system. In this perception, few authors have established a mathematical equation [8–10] and Grover's equation [11–14] to compute the MI between the inductive power pads with all type of alignments. In [15], the author has anticipated an integral equation for estimation of MI. In [16] roman et al. proposed a mathematical method to compute magnetic flux produced by the inductive power pads in the IWPT system. In [17, 18], vector potential method is developed to compute MI between inductive pad with alignments. Furthermore, in [19–21], used 3-D field method with arbitrary spatial distribution is used to compute MI flanked by inductive power pads.

The mutual inductance estimation between the square type inductive pads, assumes that square inductive pads as circular ones whose dimensions is equal to the sides of the equivalent square inductive pads. The MI for square structure is derived by multiplying MI of circular coil with $(4/\pi)^2$ [17]. When EV is at zero misalignment position i.e., receiver and transmitter inductive power pads are at same axis position, the circular structure provides good MI results, but in case of misalignment as the planar (horizontal movement of any pad) and angular (tilted angle movement of receiver pad) it will give reduced MI. The square inductive pads provide good MI results than circular inductive pads [22–24]. All these literatures require complex computations

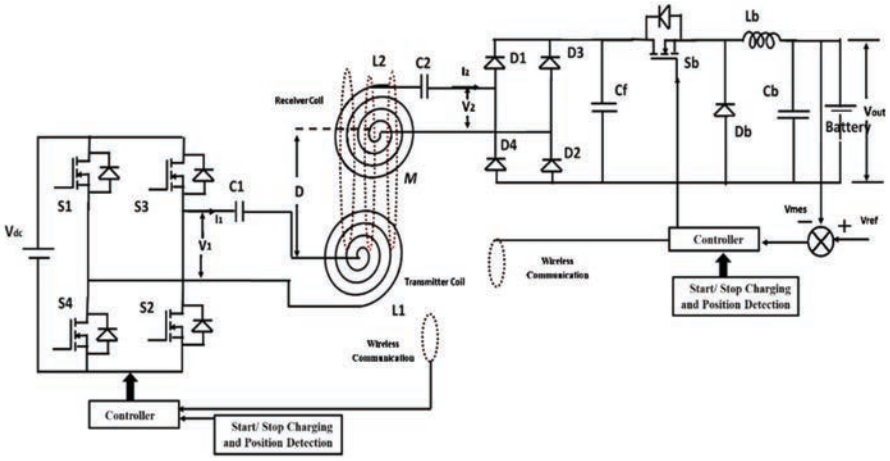

Figure 1 Graphical representation of resonant inductive WPT system.

and time-consuming process. Hence, this paper investigates the mutual inductance analysis for spiral circular and square inductive pads using FEM simulations and computed results are compared with experimental results. The schematic diagram of the IWPT of the system is shown in Figure 1.

This paper is organized as follows: the essential characteristics and mathematical modeling of the resonant IWPT system are described in Section 2. Section 3 gives FEM modelling of the IWPT inductive pads and Results obtained of mutual inductance are elaborated. Section 4 provides the analytical equations for the computation of the losses in IWPT system and experimental implementation losses, power transfer efficiency analysis is presented. Finally, the conclusion is given in Section 5.

2 Modeling of the Resonant IPT Inductive Pads

The circuit model of the IWPT system is like to the conservative transformer. Using the corresponding circuit model, as shown in Figure 2, the mathematical modelling equations of IWPT can be obtained. Assume that the transmitter is energised with alternating voltage and current under the steady-state condition. The transmitter inductive power pad parameters are R_1 (resistance), L_1 (inductance), and V_1 (inverter output voltage), I_1 (current) and of the transmitter inductive power pad parameters are R_2 (resistance), L_2 (inductance), and I_2 (current). The induced voltages in the transmitter and

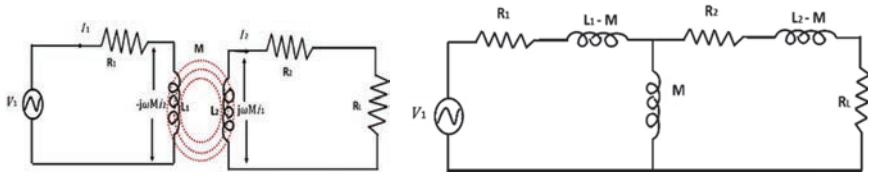

(a) (b).

Figure 2 The IWPT system's equivalent circuit model (a). Circuit with coupled coils (b). T corresponding circuit.

receiver power pads are given by

$$V_1 = j\omega L_1 I_1 + R_1 I_1 - j\omega M I_2 \tag{1}$$

$$j\omega M I_1 = j\omega L_2 I_2 + R_2 I_2 + R_L I_2 \tag{2}$$

The receiver coil current (I_2) obtained as

$$I_2 = \frac{j\omega M I_1}{Z_2} \tag{3}$$

Where $Z_2 = j\omega L_2 + R_2 + R_L$, which is the total impedance of the receiver coil and load.

$$V_1 = j\omega L_1 I_1 + R_1 I_1 + I_1 \left(\frac{\omega^2 M^2}{Z_2}\right) \tag{4}$$

$$\text{Load power} = R_L |I_2^2| = R_L \left(\frac{j\omega M I_1}{Z_2}\right)^2 \tag{5}$$

$$\text{Apparent input power} = \left\{ |j\omega L_1 + R_1| + \left(\frac{\omega^2 M^2}{Z_2}\right) \right\} |I_1^2| \tag{6}$$

$$\eta = \left(\frac{\omega^2 M^2 R_L}{\omega^2 M^2 (R_L + R_2) + R_1 (R_L + R_2)^2 + (\omega L_2)^2}\right) \tag{7}$$

From the above efficiency Equation (7) it is clear that, it will higher if the mutual inductance is high and hence, the MI play a key role.

2.1 Inductive Coil Modelling for IWPT System

The design and modelling of the inductive power pads is important because the inductive pad structures are difficult to modify once built and the typical

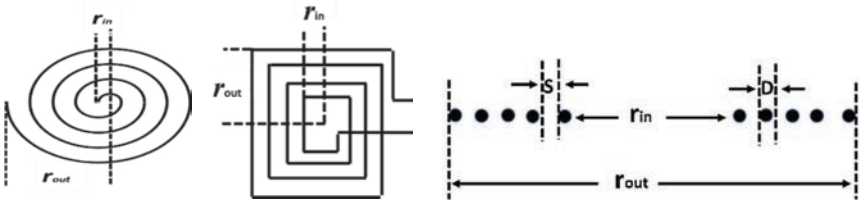

(a). (b). (c).

Figure 3 Depiction of a circular spiral inductive power pads, (a). Circular spiral inductive power pad, (b) Spiral square inductive power pad, (c). A cross-sectional view of inductive power pad.

representation of the spiral coils are shown in Figure 3. This section contains systematic equations for estimating electrical parameters inductive coils such as self-inductance and resistance. The coil design process begins with identifying the internal diameter of the coil (D_{in}). The number of turns and inner radius of the inductive pads are randomly chosen in this work.

2.2 Self-Inductance and Resistance Computation

Inductance is a proportion of the magnetic field's circulation nearby a current carrying conductor. The inductors come in a diversity of shapes and sizes. Spiral coils were used in this work for the IWPT system. The self-inductance [14–16] is calculated using the following equations.

$$L_c(\mu H) = \frac{N^2 R2}{(8R + 11W)} \tag{8}$$

$$L_{sq} = \frac{2\mu N^2 P}{\pi}\left(\ln\left(\frac{2.067}{Q}\right) + 0.17Q + 0.125Q^2\right) \tag{9}$$

Where,

R = P = $0.5(r_{out} + r_{in})$ = Mean radius of the spiral circular inductive power pad,
Q = $\frac{(r_{out} - r_{in})}{(r_{out} + r_{in})}$ = Mean radius of the spiral square inductive power pad,
W = $(r_{out} - r_{in})$ = Depth of the spiral inductive power pad.

The inner resistance of the inductive power pad is the cause of losses in the IWPT system's inductive power pads. When a conductor is provided through a high-frequency excitation, it causes the eddy current effect, skin and, proximity effects which introduces DC and AC resistance. The DC and

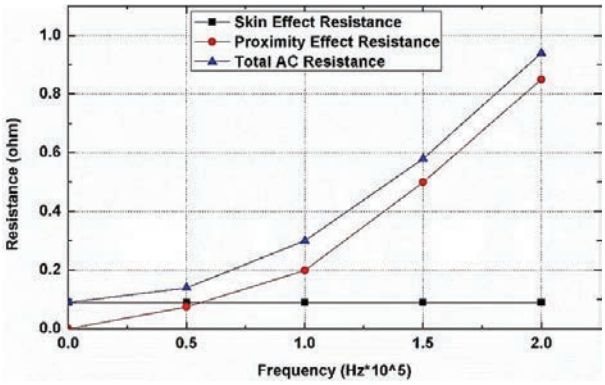

Figure 4 Litz wire AC resistance, skin effect, and proximity effect [14].

AC resistance of the inductive power pad can be calculated by the following equations [18, 19].

$$R_{dc} = \frac{4\rho_c l_{tot}}{\pi n d_s^2} \tag{10}$$

$$R_{ac} = \frac{384(8\pi f 10^{-7})R_{dc}^3}{((8\pi f 10^{-7})^2 + R_{dc}^2)^2} \tag{11}$$

The circular spiral coil's total length is given by $1 = \pi \mathrm{N}(r_{out} + r_{in})$. Where $\mathrm{r_{in}}$ and $\mathrm{r_o}$ are the inner and outer radius of the spiral circular inductive power pad.

$$r_{out}(\max) = r_{in} + N * (D + S) \tag{12}$$

$$r_{out}(\min) = r_{in} + N * D \tag{13}$$

3 Investigation of Mutual Inductance Of The Inductive Pads

3.1 Mutual Inductance of the Inductive Pads Using FEM

ANSYS Maxwell 14.0.0 3-D FEM tool has been used for computing the MI between the inductive power pads and all the imitations are performed in 2-D modelling. The inductive power pad setups established in the FEM simulation is exposed in Figure 5. The magnetic flux intensity lines at different distances are given in the following figures. The

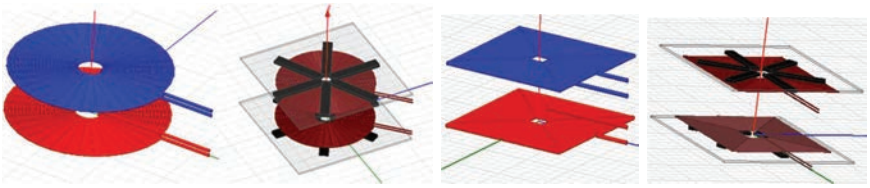

(a) (b) (c) (d)

Figure 5 FEM simulation inductive pad setups, (a). Spiral circular inductive power pads without core, (b). Spiral circular inductive power pads with core and chassis, (c). Spiral square inductive power pads without core, (b). Spiral square inductive power pads with core and chassis.

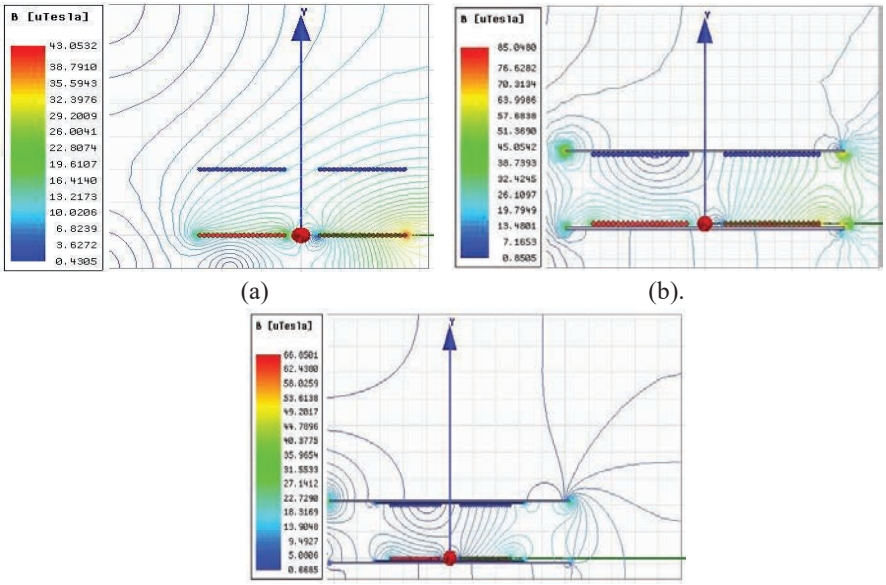

(a) (b).

(c).

Figure 6 Magnetic flux density delivery among the inductive power pads at 100 mm distance with perfect alignment, (a) With Ferrite core, (b) With Ferrite core and chassis.

Figure 6. depicts the flux density circulation among the spiral circular inductively inductive power pads at 100 mm vertical distance for different misalignments conditions. The Figure 6(a) provides magnetic flux density delivery between the spiral circular inductive pads without any core, similarly Figure 6(b), and 6(c) shows with core, with

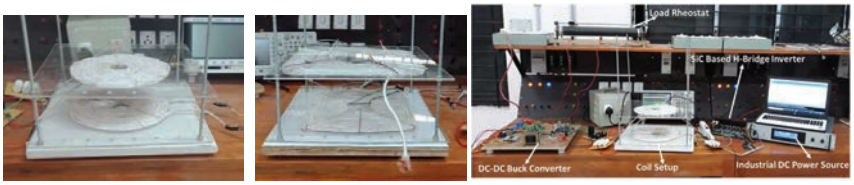

(a). (b). (c).

Figure 7 Experimental laboratory model, (a). Validated setup for WIPT system, (b). Spiral circular inductive pad setup, (c). Spiral square inductive pad setup.

core & steel chassis, respectively. It observed that the receiver inductive power pad moves away from the transmitter inductive power pad, the flux linkages will decrease as a consequence there will be reduction in MI.

3.2 Experimental Investigation of Mutual Inductance

The experimental arrangement given in Figure 7, is established for validating the MI. It consists of circular spiral inductive power pads, an Arduino microcontroller, and a MOSFET H-bridge inverter. The circular spiral coils are made up of 0.1 mm/1500 strands Litz wire and manually created misalignments of the spiral circular inductive power pads. The inverter converts DC into High-frequency (HF) AC which is fed to the inductive power pads. The open-circuit voltage (OCV) of the receiver inductive power pad at several positions are measured. The mutual inductance is calculated from the OCV [26], and it is given in Equation (15).

$$MI = \frac{V_{2oc}}{\omega MI_1} \tag{14}$$

3.3 Mutual Inductance Analysis

The MI values are graphically denoted in Figure 8 for all possible positions without core environment. Hereby taking the vertical distance (VD) as a parameter, the MI values are analyzed for all misalignments of the inductive power pads. The VD is speckled from 0 to 200 mm. From Figure 8 the Mutual inductance is high in spiral square pads compare to spiral circular pads in all misalignment conditions. Tables 1 and 2 provides the MI values of spiral circular and spiral square inductive pads with core at various angular misalignments (AM) depict for the inductive pads. The results FR indicates the finite element modelling values, and ER presents the experimental values.

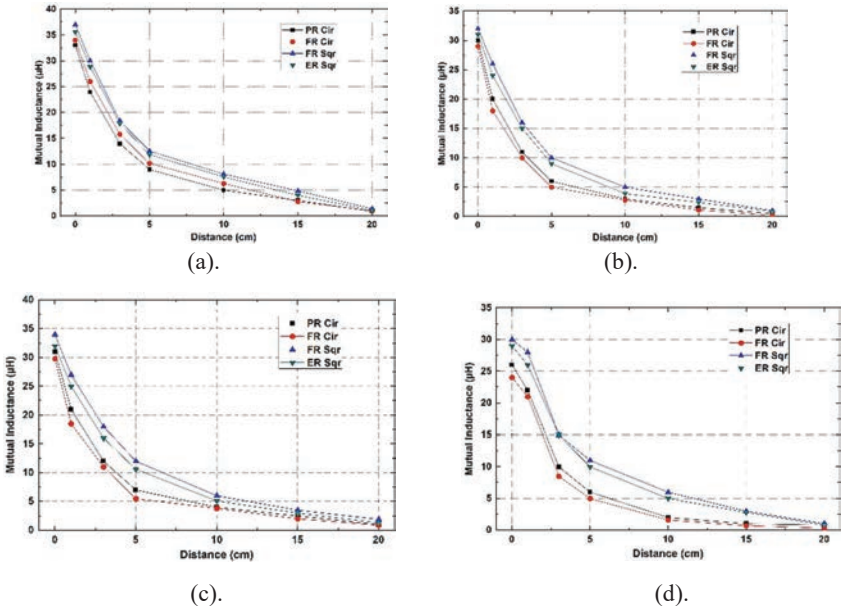

Figure 8 Mutual inductance without core (a). 0 mm horizontal misalignment, (b). 50 mm horizontal misalignment, (c). 15° angular misalignment, (d). 45° angular misalignment.

Table 1 MI Values at 0 mm horizontal misalignment with ferrite core for spiral square pads

	0 mm Horizontal Misalignment							
Vertical	AM (0°)		AM (15°)		AM (30°)		AM (45°)	
Distance (mm)	FER	ER	FER	ER	FER	ER	FER	ER
25	56.26	53.23	52.27	50.05	51.21	48.45	47.15	45.85
50	53.41	51.05	51.13	48.12	48.29	45.43	45.21	42.65
75	50.89	47.71	48.01	45.47	45.53	42.82	41.54	38.12
100	40.89	37.61	35.32	32.47	33.68	31.32	28.78	24.98
125	28.65	26.21	25.14	23.65	22.56	21.41	19.29	16.56
150	23.53	20.24	19.45	16.55	17.12	14.78	11.89	8.12
175	20.47	17.45	15.13	13.65	12.59	10.54	8.86	6.67
200	17.21	15.78	14.10	11.28	10.57	9.23	7.41	5.30

4 Losses in Series/Series Resonant IWPT System

4.1 Power Converter Losses

The power loss in the resonant IPT system consist of loss due to high frequency (HF) inverter coil loss, DC-DC converter and diode bridge rectifier

Table 2 MI Values at 0 mm horizontal misalignment with ferrite core for spiral circular pads

Vertical	0 mm Horizontal Misalignment							
	AM (0°)		AM (15°)		AM (30°)		AM (45°)	
Distance (mm)	FER	ER	FER	ER	FER	ER	FER	ER
25	53.32	52.12	50.45	48.63	47.23	44.51	43.12	38.74
50	52.54	49.55	48.65	45.34	44.12	41.61	40.43	35.40
75	49.41	46.49	46.11	43.51	42.31	39.14	37.84	33.24
100	39.65	36.65	35.12	32.54	30.44	27.43	26.78	23.75
125	27.56	24.85	23.14	20.41	18.65	15.44	14.55	12.44
150	22.54	19.57	17.56	14.57	13.74	10.54	9.44	7.64
175	20.14	17.84	16.77	12.22	12.45	8.27	7.37	5.22
200	17.73	15.22	14.31	11.47	10.54	7.41	6.46	4.11

loss. The HF inverter switches produce conduction and switching losses during its operation. The analytical calculation of the inverter MOSFET switch conduction and switching losses can be computed using Equations (15) and (16) respectively. The body diode of the MOSFET also products reverse recovery losses (P_{rr}) and conduction losses (P_{CD}), their respective equations are given in Equations (17) and (18).

$$P_{Cmos} = I_{mos}^2 r_{dson} \tag{15}$$

$$P_{sw} = \frac{1}{2} I_{mosoff}(\mathrm{t}_{ri} + \mathrm{t}_{fu})\mathrm{V}_{sw} f_{sw} \tag{16}$$

$$P_{CD} = V_f I_{DRMS} \tag{17}$$

$$P_{rr} = \frac{1}{4} Q_{rr} V_{dc} f_{sw} \tag{18}$$

Where, I_{mos} is RMS value of the MOSFET forward current, I_{mosoff} is the MOSFET current while turn off, r_{dson} is MOSFET drain to source ON state resistance. In the operation of high-frequency inverter for cycle two MOSFET conduct at a time. Hence, the total MOSFET losses can be calculated as:

$$P_{total} = 2(P_{Cmos} + P_{sw} + P_{CD} + P_{rr}) \tag{19}$$

The receiver side of the resonant IWPT system consists of a diode bridge and DC-DC buck converter; hence these two converters produce losses. The diode bridge rectifier produces reverse recovery and conduction loss. The reverse recovery losses will be zero because the diodes will be turned ON

and OFF at zero current. The conduction losses of the rectifier are given by Equation (20)

$$P_{rect} = V_{fr} I_{rect} \tag{20}$$

where I_{rect} is the current flowing through diodes and V_{fr} is the forward voltage drop across the diode.

The losses in the DC-DC buck converter are the sum of loss in the inductor and semiconductor switch loss.

$$\begin{aligned} P_{buck} &= P_C + P_S + P_L + P_{coreL} \\ &= I_{bmos}^2 r_{dson} + \frac{1}{2} I_{bmosoff}(t_{ri} + t_{fu}) V_{sw} f_{sw} + Q_{rr} V_{dc} f_{sw} \\ &\quad + \frac{1}{2} I_{Bmosoff}(t_{ru} + t_{fi}) + \frac{1}{4} Q_{rr} V_{dc} f_{sw} + I_{Lbuck}^2 r_{dson} \end{aligned} \tag{21}$$

4.2 Inductive Pad (Coil) Losses

Three different losses occur in inductive pads such as skin effect losses, Proximity losses and core losses. The system's operating frequency is in the kHz range. The skin effect becomes noticeable at these frequencies, and hence the losses can be computed calculated using following equations,

$$P_{skin} = n\, R_{dc} k(f_o) \left(\frac{\hat{I}}{n} \right)^2 \tag{22}$$

$$P_p = R_{dc} k_p(f_o) \widehat{H_e^2} \tag{23}$$

$$P_{core} = k\, f_o^{\alpha} B^{\beta} \tag{24}$$

where H_{e} is the peak value of the magnetic field and k, α, β are the Steinmetz parameters of the core material.

4.3 Loss Analysis in Experimental Resonant IWPT System

The total loss in the series resonant IWPT system is calculated by measuring power at each stage of the system. Figure 9 provides total losses of the system at different losses, and from the figure, it is clear that as misalignment distance increases total power losses in the system increases hence, which results in the reduction of the overall efficiency of the system. Figures 9(a) and 9(b) shows the series IWPT system losses at spiral circular and square structure, respectively.

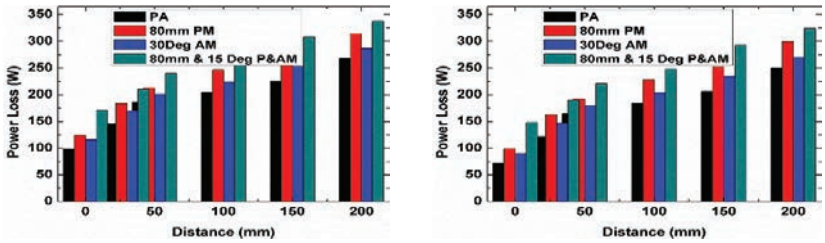

Figure 9 Bar diagram loss analysis of the resonant IWPT system with different misalignment, (a) circular structure, (b) square structure.

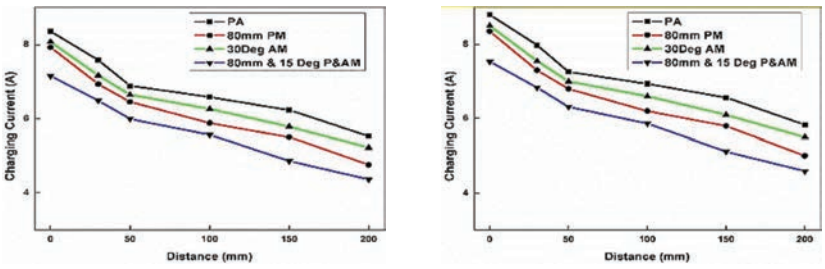

Figure 10 Series resonant IWPT battery charging current at different misalignment, (a) circular structure, (b) square structure.

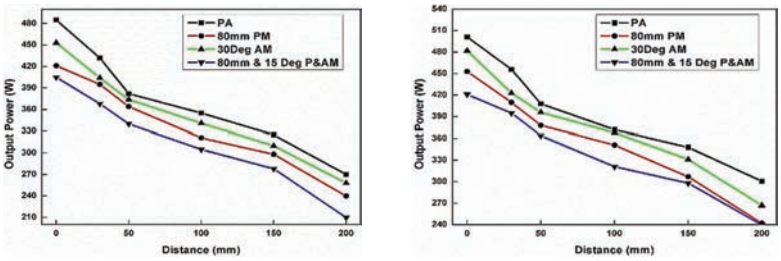

Figure 11 Series resonant IWPT battery charging power at different misalignment, (a) circular structure, (b) square structure.

4.4 Analysis of Battery Charging Voltage, Current and Overall System Efficiency

The output battery charging voltage is maintained at a constant 60 volts. The current and power analysis of the series resonant IWPT system is shown in Figures 10 and 11, respectively. It is clear that at perfect alignment, the

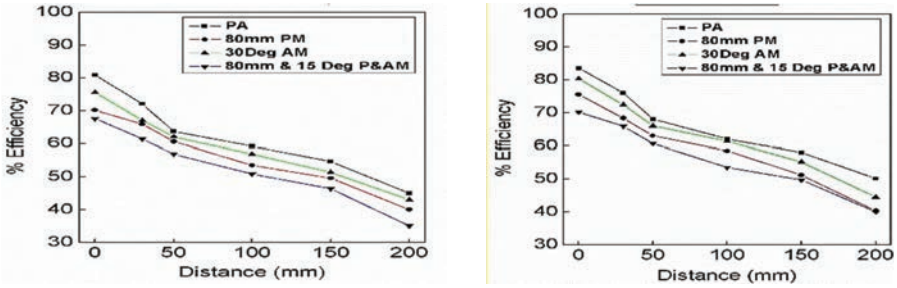

(a) (b).

Figure 12 Overall efficiency (DC-DC) vs distance between the coupled coils with different misalignments at, (a) circular structure, (b) square structure.

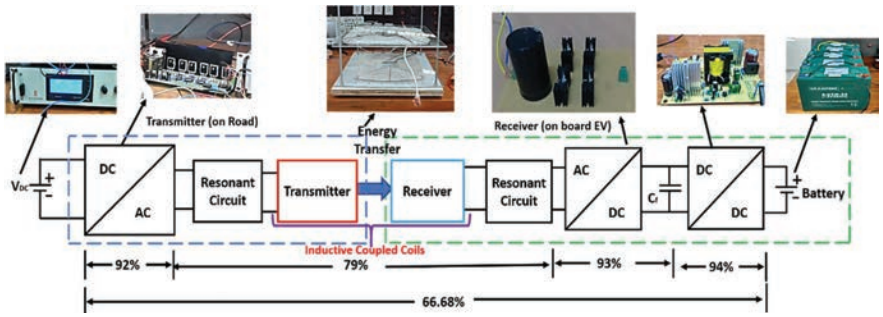

Figure 13 Representation of the overall efficiency (DC-DC) of series resonant IWPT system at 100 mm vertical distance 0 mm horizontal alignment with square structure.

system is supplying the charging current with square coupled inductive power pad to the battery is 8.6 A. The output power at different misalignments of the system is presented in Figure 10. The overall system efficiency is shown in Figure 12. However, the prototype system was built, as proof of concept, using comparatively at low output, input voltages. Subsequently, the efficiency that was achieved in the sample system is quite low. The measured overall DC-DC efficiency of the proposed system at different misalignments and different vertical displacement condition is shown in Figures 12(a) and 12(b) respectively for circular and square structures. Figure 13 shows the individual components and over the efficiency of the series resonant IWPT system at 100 mm vertical distance and perfectly aligned square inductive coupled coils of the system.

Table 3 Parameters of the system

Parameter		Specification
Number of turns	Circular Coil	20
Coil Diameter		26 cm
Inner Radius of the coil		4 cm
Conductor Diameter		0.55 cm
Self-inductance of circular coil		56.46 μH
Internal Resistance of circular coil		0.4 Ω
Number of turns	Square Coil	20
Inner Length		4 cm
Conductor Radius		0.55 cm
Self-inductance of square coil		80.05 μH
Internal Resistance of square coil		0.321 Ω

5 Conclusions

The implementation of series resonant IWPT system with the circular and square structure for EV battery charging is analyzed. The coupling characteristics of spiral circular and square inductive pads of the system are investigated. The battery charging current and battery charging power at different misalignments are described, and the power loss analysis of the resonant IWPT system is also provided. From the analysis, it is vibrant that the movements between the coil increases the charging current decreases which results in a reduction of charging power, hence the charging time of the battery increases.

References

[1] M. Yilmaz and P. T. Krein, "Review of battery charger topologies, charging power levels, and infrastructure for plug-in electric and hybrid vehicles," *IEEE Transactions Power Electronics*, 28(5), pp. 2151–2169, May 2013.

[2] A. Emadi, M. Ehsani, and J. M. Miller, Eds., Vehicular Electric Power Systems: Land, Sea, Air, and Space Vehicles. Boca Raton, FL, USA: CRC Press, 2003.

[3] Siqi Li and Chunting Chris Mi "Wireless Power Transfer for Electric Vehicle Applications" *IEEE Journal of Emerging and Selected Topics in Power Electronics*, 3(1), 4–17, 2015.

[4] Young K., Wang C, Le Yi Wang, and Strunz K., (2012) "Chapter 2: Electric Vehicle Battery Technologies", from the book "Electric Vehicle Integration into Modern Power Networks" Springer

[5] Bosshard and J. W. Kolar, "Inductive power transfer for electric vehicle charging: Technical challenges and tradeoffs," in *IEEE Power Electronics Magazine*, 3(3), pp. 22–30, Sept. 2016.

[6] D. Patil, M. K. McDonough, J. M. Miller, B. Fahimi and P. T. Balsara, "Wireless Power Transfer for Vehicular Applications: Overview and Challenges," in *IEEE Transactions on Transportation Electrification*, 4(1), pp. 3–37, March 2018.

[7] Khaligh A., and Dusmez S., "Comprehensive Topological Analysis of Conductive and Inductive Charging Solutions for Plug-In Electric Vehicles" *IEEE Transactions Vehicular Technology*, 61(8), 2012, 3475–3489.

[8] M. Vinod, D. Kishan, N. Harishchandrappa and B. D. Reddy, "Comparative Analysis of Symmetrical and Asymmetrical Phase Shift Control Strategy for Resonant Wireless Inductive Charging System," *2021 IEEE International Power and Renewable Energy Conference (IPRECON)*, 2021, pp. 1–6.

[9] Zhicong Huang, Siu-Chung Wong, and Chi K. Tse (2016) "Design of a Single-Stage Inductive-Power-Transfer Converter for Efficient EV Battery Charging" *IEEE Transactions on Vehicular Technology*, 66(7), 5808–5821.

[10] Y. Liu, U. K. Madawala, R. Mai and Z. He, "Zero-Phase-Angle Controlled Bidirectional Wireless EV Charging Systems for Large Coil Misalignments," in *IEEE Transactions on Power Electronics*, vol. 35, no. 5, pp. 5343–5353, May 2020.

[11] Kunwar Aditya and Sheldon S. Williamson, "A Review of Optimal Conditions for Achieving Maximum Power Output and Maximum Efficiency for a Series–Series Resonant Inductive Link" *IEEE Transactions on Transportation Electrification*, 3(2), 2017, 303–311.

[12] D. Kishan, M. Vinod and N. Harischandrappa, "Magnetic Coupling Characteristics of Spiral Square - Circular Coupled Coils for Wireless EV Battery Charging System," *2020 IEEE 17th India Council International Conference (INDICON)*, 2020, pp. 1–5.

[13] Sándor Bilicz, Zsolt Badics, Szabolcs Gyimóthy, and József Pávó "Modeling of Dense Windings for Resonant Wireless Power Transfer by an Integral Equation Formulation". *IEEE Transactions On Magnetics*, 2017, 53(6).

[14] J. Acero, C. Carretero, I. Lope, R. Alonso, O. Lucia, and J. M. Burdio, "Analysis of the Mutual Inductance of Planar-Lumped Inductive Power Transfer Systems," *IEEE Trans. on Industrial Electronics.*, 2013, 60, pp. 410–420.

[15] L. Huang, G. Meunier, O. Chadebec, J. M. Guichon, Y. Li and Z. He, "General Integral Formulation of Magnetic Flux Computation and Its Application to Inductive Power Transfer System," in *IEEE Transactions on Magnetics*, 2017, 53(6), pp. 1–4.

[16] Weihan li, Han zhao, Junjun Deng, Siqi Li, Chunting Chris Mi. "Comparison Study on SS and Double-Sided LCC Compensation Topologies for EV/PHEV Wireless Chargers," *IEEE Transactions on Vehicular Technology*, Vol: 65, Issue: 6, pp. 4429–4439, 2016.

[17] Ezhil Reena Joy, Brijesh Kumar, Gautam Rituraj, Praveen Kumar "Analysis and comparison of four compensation topologies of contactless power transfer system" *2015 4th International Conference on Electric Power and Energy Conversion Systems* (EPECS).

[18] Wei-Cheng Wang, Cheng-Chi Tai, ShengJie Wu, and Zih-Yi Liu. "A hybrid genetic algorithm with fuzzy logic controller for wireless power transmission system of electric vehicles", *2015 IEEE International Conference on Industrial Technology* (ICIT), 2015.

[19] Xiaohui Qu, Yanyan Jing, Hongdou Han, Siu-Chung Wong and Chi K. Tse "Higher Order Compensation for Inductive-Power-Transfer Converters With Constant-Voltage or Constant-Current Output Combating Transformer Parameter Constraints" *IEEE Transactions On Power Electronics*, Vol. 32, No. 1, 2017.

[20] Zhang, Wei, Siu-Chung Wong, Chi K. Tse, and Qianhong Chen. "Analysis and Comparison of Secondary Series- and Parallel-Compensated Inductive Power Transfer Systems Operating for Optimal Efficiency and Load-Independent Voltage-Transfer Ratio", *IEEE Transactions on Power Electronics*, Vol: 29, Issue: 6, pp. 2979–2990, 2014.

[21] H. V. Alizadeh and B. Boulet, "Analytical calculation of the magnetic vector potential of an axisymmetric solenoid in the presence of iron parts," IEEE Trans. Magnetics, Vol. 52, 2016.

[22] S. I. Babic and C. Akyel, "New analytic-numerical solutions for the mutual inductance of two coaxial circular coils with rectangular cross section in air," IEEE Trans. Magn., vol. 42, no. 6, pp. 1661–1669, Jun. 2006.

[23] J. T. Conway, "Analytical solutions for the self- and mutual inductances of concentric coplanar disk coils," IEEE Trans. Magn., vol. 49, no. 3, pp. 1135–1142, Mar. 2013.

[24] C. P. Yue and S. Wong, "Physical modeling of spiral inductors on silicon," *IEEE Trans. Electron Devices*, vol. 47, no. 3, pp. 560–568, Mar. 2000.

[25] S. S. Mohan, M. del Mar Hershenson, S. P. Boyd, and T. H. Lee, "Simple accurate expressions for planar spiral inductances," *IEEE J. Solid-State Circuits*, vol. 34, no. 10, pp. 1419–1424, Oct. 1999.

[26] P Srinivasa Rao Nayak, Dharavath Kishan, P Sathish "Investigation of Mutual Inductance between Circular Spiral Coils with Misalignments for Electric Vehicle Battery Charging" *IET Science, Measurement & Technology*, Vol. 12, No. 7, pp. 844–850, Oct. 2018.

[27] A. Ramezani and M. Narimani, "Optimal Design of Fully Integrated Magnetic Structure for Wireless Charging of Electric Vehicles," in *IEEE Transactions on Transportation Electrification*, vol. 7, no. 4, pp. 2114–2127, Dec. 2021.

[28] M. Zucca, P. Squillari and U. Pogliano, "A Measurement System for the Characterization of Wireless Charging Stations for Electric Vehicles," in *IEEE Transactions on Instrumentation and Measurement*, vol. 70, pp. 1–10, 2021.

[29] P. K. Joseph, D. Elangovan and P. Sanjeevikumar, "System Architecture, Design, and Optimization of a Flexible Wireless Charger for Renewable Energy-Powered Electric Bicycles," in IEEE Systems Journal, vol. 15, no. 2, pp. 2696–2707, June 2021.

Biography

Dharavath Kishan received the B. Tech degree in Electrical and Electronics Engineering and M. Tech degree in Power Electronics from Jawaharlal Nehru Technological University Hyderabad respectively in 2011 and 2013 and he received his PhD degree from National Institute of Technology Tiruchirappalli in 2018. Currently he is working as Assistant Professor in Department of E & E Engineering at National Institute of Technology Karnataka (NITK), Surathkal, India. Prior to joining NITK he worked as Assistant Professor at Faculty of Science and Technology, IFHE Hyderabad. Dr Kishan current research interests include power electronics and its applications in electric vehicles, wireless power transfer and transportation electrification. He has published 16 research papers in reputed journals and peer reviewed international conferences. He is also delivered guest lectures at various events on Wireless Power Transfer for electric vehicles. He is also an IEEE Senior Member and IAS, PELS & IES Society member. Dr Kishan is also an active reviewer for various reputed IEEE transactions like IEEE Transactions on Electromagnetic compatibility, IEEE Transactions on Industrial Electronics, IEEE Transactions on vehicular Technology, and IEEE Access, IET Renewable Power Generation. He has guided two master level students in the area of power electronics and currently guiding one master and Five PhD students in the area of Power Electronic Applications.